Cell Host & Microbe
Article

# Entrapment of Intracytosolic Bacteria by Septin Cage-like Structures

Serge Mostowy,[1,6,7,*] Matteo Bonazzi,[1,6,7] Mélanie Anne Hamon,[1,6,7] To Nam Tham,[1,6,7] Adeline Mallet,[2] Mickaël Lelek,[3,8] Edith Gouin,[1,6,7] Caroline Demangel,[4] Roland Brosch,[4] Christophe Zimmer,[3,8] Anna Sartori,[2] Makoto Kinoshita,[9] Marc Lecuit,[5,10,11] and Pascale Cossart[1,6,7,*]
[1]Unité des Interactions Bactéries-Cellules
[2]Imagopole, Ultrastructural Microscopy Platform
[3]Groupe Imagerie et Modélisation
[4]Unité Postulante Pathogénomique Mycobactérienne Intégrée
[5]Groupe Microorganismes et Barrières de l'Hôte
Institut Pasteur, Paris F-75015, France
[6]Inserm, Unité 604, Paris F-75015, France
[7]Institut National de la Recherche Agronomique, Unité Sous Contrat 2020, Paris F-75015 France
[8]Centre National de la Recherche Scientifique, Unité de Recherche Associée 2582, Paris F-75015, France
[9]Department of Molecular Biology, Division of Biological Sciences, Nagoya University Graduate School of Science, Nagoya 464-8602, Japan
[10]Inserm, Avenir, Unité 604, Paris F-75015, France
[11]Université Paris Descartes, Centre d'Infectiologie Necker-Pasteur, Service des Maladies Infectieuses et Tropicales, Hôpital Necker-Enfants malades, Assistance Publique-Hôpitaux de Paris, Paris F-75015, France
*Correspondence: smostowy@pasteur.fr (S.M.), pcossart@pasteur.fr (P.C.)
DOI 10.1016/j.chom.2010.10.009

## SUMMARY

**Actin-based motility is used by various pathogens for dissemination within and between cells. Yet host factors restricting this process have not been identified. Septins are GTP-binding proteins that assemble as filaments and are essential for cell division. However, their role during interphase has remained elusive. Here, we report that septin assemblies are recruited to different bacteria that polymerize actin. We observed that intracytosolic *Shigella* either become compartmentalized in septin cage-like structures or form actin tails. Inactivation of septin caging increases the number of *Shigella* with actin tails and enhances cell-to-cell spread. TNF-α, a host cytokine produced upon *Shigella* infection, stimulates septin caging and restricts actin tail formation and cell-to-cell spread. Finally, we show that septin cages entrap bacteria targeted to autophagy. Together, these results reveal an unsuspected mechanism of host defense that restricts dissemination of invasive pathogens.**

## INTRODUCTION

The actin cytoskeleton is exploited by several bacterial pathogens, including *Listeria monocytogenes* and *Shigella flexneri*, for their own intra- and intercellular motility (Gouin et al., 2005). The Arp2/3 complex activates the nucleation of actin polymerization and induces the formation of a highly branched actin filament network in pathogen actin tails and lamellipodia (Pollard and Borisy, 2003). Arp2/3 has to be activated by various proteins including the WASP/N-WASP/Scar/WAVE family in eukaryotic cells or by the ActA protein at the surface of *L. monocytogenes* (Pollard and Borisy, 2003). The *Shigella* protein IcsA is not directly involved in the activation of actin nucleation but instead recruits N-WASP and then Arp2/3 (Suzuki et al., 1998). Despite major advances in our understanding of actin-based motility of cells and pathogens in vitro, a complete picture of proteins and mechanisms regulating actin dynamics and movement in vivo has not been obtained. This may be critical for the complete understanding of infectious processes.

Once invasive bacteria reach the cytosol, they can encounter the innate surveillance system of autophagy (Levine and Deretic, 2007; Münz, 2009). Autophagy is an evolutionarily conserved catabolic pathway that allows eukaryotes to degrade and recycle intracellular components by sequestering proteins and organelles in specialized double-membrane vesicles named autophagosomes (Yang and Klionsky, 2010). To study its function in diverse biological processes, methods to monitor autophagy and to modulate autophagic activity are well established (Mizushima et al., 2010). Recent evidence has implicated the autophagic pathway in pathogenesis (Levine and Deretic, 2007), and ubiquitylation has emerged as central for autophagic recognition of intracytosolic pathogens (Thurston et al., 2009; Yoshikawa et al., 2009)—i.e., ubiquitin-associated bacteria are recognized by the autophagy machinery and become trapped by autophagosomal membrane as a prelude for delivery to lysosomes for degradation. However, different pathogens have evolved several ways to escape autophagy (Deretic and Levine, 2009). For example, *Listeria* can evade autophagic recognition by expressing the surface protein ActA (Yoshikawa et al., 2009). Alternatively, *Shigella* avoids the autophagic response via the bacterial effector protein IcsB, which prevents the recruitment of Atg5, a protein critical for autophagome maturation, to IcsA (Ogawa et al., 2005). Thus, both *Listeria* ActA and *Shigella* IcsA play key roles in actin polymerization and autophagosome formation.

Septins are conserved GTP-binding proteins discovered in *Saccharomyces cerevisiae*, where they organize as a ring at the bud neck (Byers and Goetsch, 1976; Hartwell, 1971). The 14 human septins can be subdivided into four groups on the basis of sequence homology, and septins from different groups interact to generate hetero-oligomeric complexes that form nonpolar filaments (Sirajuddin et al., 2007) and associate with cellular membranes, actin filaments, and microtubules (Kinoshita, 2006; Spiliotis and Nelson, 2006). Septins play key roles in cell division, cytoskeletal dynamics, and membrane remodeling (Hall et al., 2009), and their dysfunction has been implicated in the pathogenesis of various diseases including cancer (Hall and Russell, 2004), hereditary neuralgic amyotrophy (Kuhlenbäumer et al., 2005), and Parkinson's disease (Ihara et al., 2007). Beyond insights gained by the recent crystal structure of a septin complex (Sirajuddin et al., 2007; Weirich et al., 2008), how septins behave as an unconventional component of the cytoskeleton remains poorly understood. We recently reported that septin collars, similar to those originally described at the yeast bud neck, are formed at sites of bacterial entry into mammalian nonphagocytic cells (Mostowy et al., 2009b). Cells treated with cytochalasin D do not recruit septin at the phagocytic cup (Huang et al., 2008; Mostowy et al., 2009b), suggesting that the accumulation of septins is intimately linked to the accumulation of actin, albeit in an unknown fashion. While instrumental for bacterial entry (Mostowy et al., 2009a; Mostowy et al., 2009b), the role of septins during other actin-based infection strategies has not been investigated. In the current study, we identify septin caging as a mechanism of host defense that controls the fate of intracytosolic bacteria toward intercellular spread or autophagy.

## RESULTS

### Septin Rings Assemble at Sites of Actin Polymerization

We first addressed whether septin rings similar to those detected during the entry process (Mostowy et al., 2009b) assemble during the actin-based motility of *Listeria* and *Shigella*. SEPT2 rings formed around *L. monocytogenes* actin tails and surrounded also bacterial bodies (Figure 1A). A similar assembly was observed for two SEPT2-binding partners (Mostowy et al., 2009b), SEPT9 (Figure 1A) and SEPT11 (data not shown). Septin rings also formed around actin tails and bodies of *Listeria ivanovii* (Figure 1B) and *S. flexneri* (Figure 1C). Septin recruitment to *Listeria* and *Shigella* actin tails was confirmed using real-time microscopy with fluorescent septin constructs, although the ring-like structures were more difficult to discern (Movie S1 available online).

Septin recruitment was visible for 23% ± 7% (*Listeria*) or 28% ± 2% (*Shigella*) of actin tails (mean ± standard error of the mean [SEM] from n = 3 and 6 experiments, respectively). To investigate whether septin recruitment to the actin tail plays a regulatory role, we measured actin-based velocity in control cells or in cells depleted of SEPT2 or SEPT9. SEPT6 group members have been reported to compensate for SEPT11 depletion (Mostowy et al., 2009a; Hanai et al, 2004; Ono et al., 2005), and thus functional analysis of SEPT11 was not considered here. Intracytosolic *Listeria* or *Shigella* moved at 7.8 ± 0.5 μm/min or 19.1 ± 1.6 μm/min in control cells, respectively, and similar values were observed in septin-depleted cells (Figures 1D and 1E). Together, these data suggest that septin recruitment inside cells does not modulate movement, in agreement with the fact that septins were not among the proteins identified as essential for actin-based motility in vitro or in cellular extracts (Loisel et al., 1999; Van Troys et al., 2008). Importantly, *L. monocytogenes* EGDΔ*actA* and *S. flexneri* M90TΔ*icsA*, i.e., isogenic mutant strains unable to polymerize actin in the cytosol of cells, both failed to recruit septin (Figures S1A and S1B). Therefore, septin rings assemble at sites of actin polymerization and depend on actin polymerization.

### Septins Form Cages around Intracytosolic Bacteria

Strikingly, intracytosolic *Shigella* having polymerized an actin cloud, though without an actin tail, were also surrounded by SEPT2, SEPT9, and SEPT11 collar-shaped structures. Septin recruitment to intracytosolic nonmotile *Listeria* was difficult to characterize, and complete septin rings were rarely observed (Figure S2A). In contrast, septin cage-like structures completely enveloped *Shigella* devoid of actin tails (Figure 2A), and approximately 15%–30% of intracytosolic *Shigella* were compartmentalized in septin cages at any given time (described below, Figure 2E). Three-dimensional confocal reconstruction showed that septin rings were detectable next to actin around the bacterium, with septin capping the bacterial poles (Movie S2). Stochastic optical reconstruction microscopy (STORM) was used to obtain a high-resolution image of fluorescently labeled assemblies and showed that ~0.1 μm (thick) septin structures assembled into ~3.0 μm × 0.9 μm (length × width) cages around individual *Shigella* (Figure 2B). To further characterize the ultrastructure of septin cages compartmentalizing *Shigella*, we used correlative light-scanning electron microscopy (CL-SEM) and immunogold labeling for different septins (i.e., SEPT2 and SEPT6) (Figure S2B). Septin filamentous assemblies were detected as bundles around the bacterium (Figure S2C). As septin cages were clearly identified in cells infected with *Shigella*, we focused on *Shigella* to analyze more precisely their formation.

N-WASP is recruited by IcsA to the *Shigella* poles during actin-based motility (Suzuki et al., 1998) and was detected at *Shigella*-septin cages (Figure 2C). As observed for actin (Figure 2A), N-WASP did not colocalize with septin. Depletion of N-WASP by small interfering RNA (siRNA) significantly reduced the number of *Shigella*-septin cages (4.8- ± 1.0-fold, Figure 2D), in agreement with the data that actin polymerization is critical for septin recruitment. To investigate the function of septin cages, we first counted the proportion of *Shigella*-septin cages and actin tails during the course of infection (Figure 2E). At 1 hr 40 min after infection, we observed that 29% ± 4% of *Shigella* were compartmentalized in septin cages and 24% ± 4% had actin tails. When infection was extended to 6 hr 40 min, 16% ± 2% of *Shigella* were still in septin cages, whereas only 4% ± 1% had actin tails. Thus, the proportion of *Shigella*-septin cages over actin tails persisted during the course of infection. Septin assembly was then followed with video microscopy and fluorescent septin constructs (Movie S3). Cage-like structures were observed to compartmentalize nonmotile *Shigella* for several hours (S.M. and P.C., unpublished data). We thus performed fluorescence recovery after photobleaching (FRAP) to investigate the turnover of septins that localize to the *Shigella*-septin cage. The

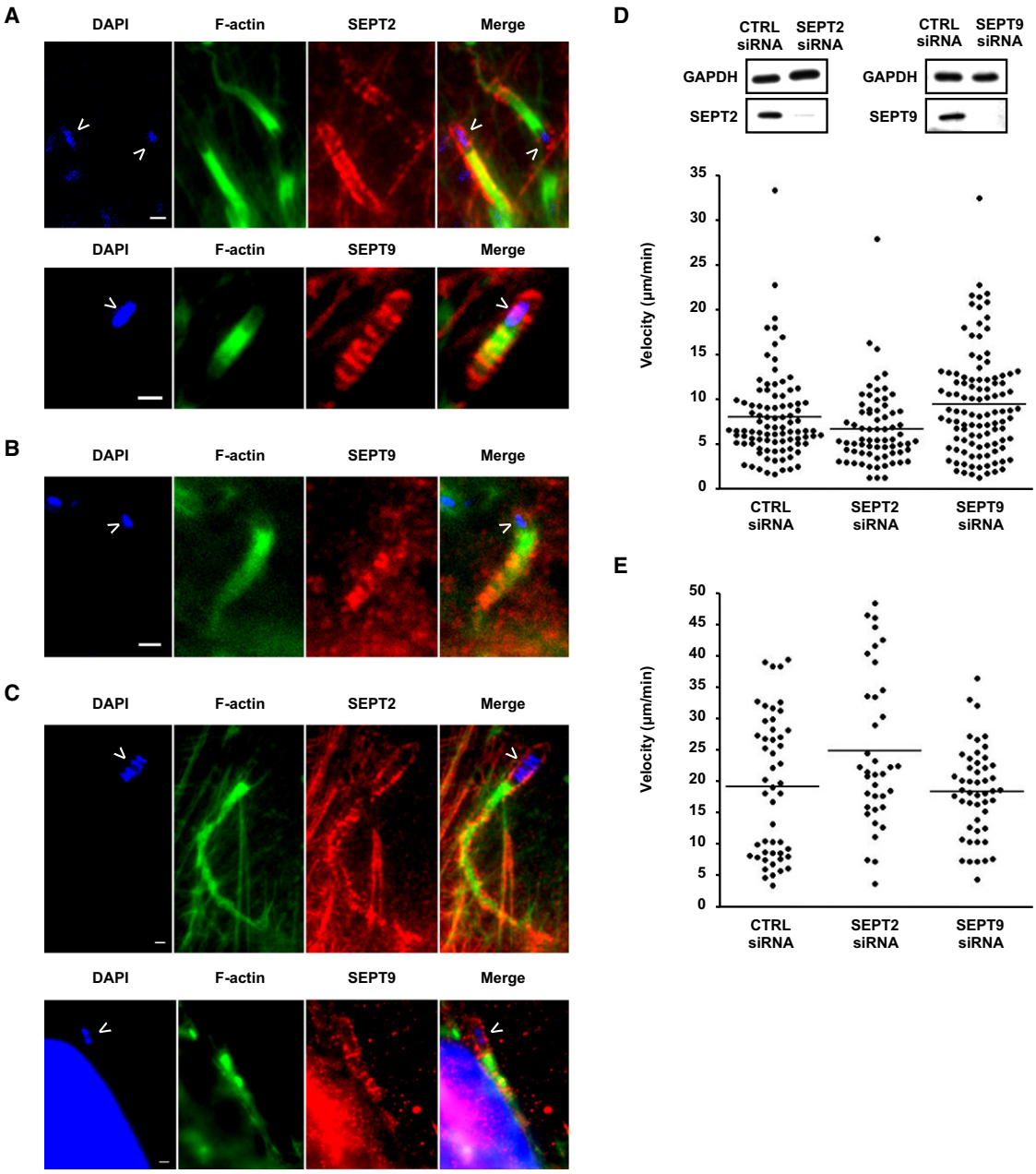


**Figure 1. Septin Rings are Recruited to Actin Tails**

(A–C) HeLa cells were infected with *L. monocytogenes* (A), *L. ivanovii* (B), or *S. flexneri* (C) for 3–5 hr, fixed for fluorescent light microscopy, and stained with phalloidin and antibodies to SEPT2 or SEPT9. White arrowheads point to motile bacterium. Scale bars represent 1 μm. Similar images were obtained labeling for SEPT11.

(D and E) HeLa cells were treated with control (CTRL), SEPT2, or SEPT9 siRNA. Whole-cell lysates of siRNA-treated cells were immunoblotted for GAPDH, SEPT2, or SEPT9 to show the efficiency of septin depletion (D, top). After 2 hr of infection, *Listeria* (D, bottom) or *Shigella* (E) velocity in siRNA-treated cells was quantified. Each dot represents the velocity of a motile bacterium polymerizing actin.

See also Figure S1 and Movie S1.

fluorescence of SEPT2-YFP or SEPT6-GFP did not reappear after photobleaching (Figures S2D and S2E; Movie S4), confirming that septin cages compartmentalizing *Shigella* are stable.

We next examined septin cages by real-time video microscopy. Septin cages formed after an initial phase of actin polymerization (Movies S5 and S6), raising the possibility that septin caging prevents actin tail formation. To test this hypothesis, we assessed the impact of septin disruption on the proportion of motile bacteria. We treated cells with control or SEPT2 siRNA and infected these cells with *Shigella*. After fixation, fluorescent light microscopy was used to compare the number of *Shigella*-septin cages and actin tails in siRNA-treated cells.

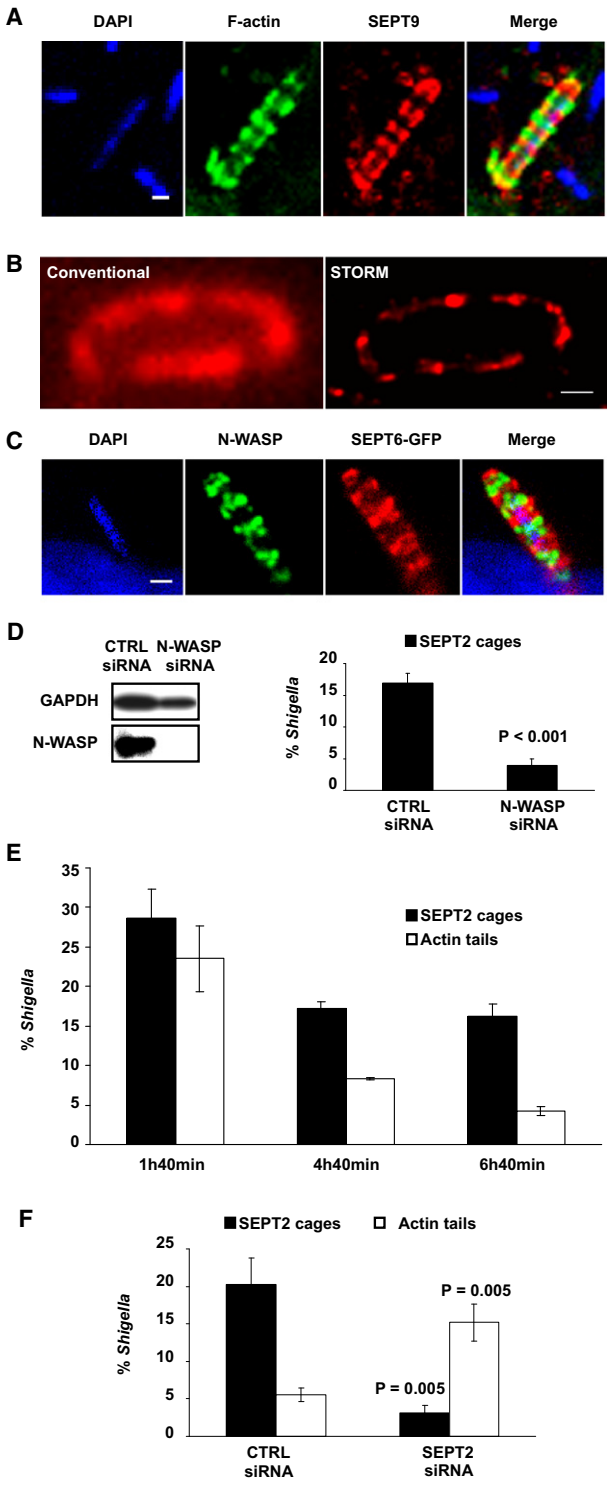


**Figure 2. The *Shigella*-Septin Cage**

(A) HeLa cells were infected with *S. flexneri* for 4 hr 40 min, fixed for confocal microscopy, and stained with phalloidin and antibodies to SEPT9. The scale bar represents 1 μm. Similar images were obtained labeling for SEPT2 or SEPT11.

(B) HeLa cells were infected with *S. flexneri* for 4 hr 40 min, fixed for STORM, and stained with antibodies to SEPT2. A conventional (left) and STORM (right) image of a *Shigella*-septin cage is shown. The scale bar represents 0.5 μm. Similar images were obtained labeling for SEPT9 or with SEPT9-mEOS2.

SEPT2-depleted cells had significantly fewer cages (10.0- ± 6.0-fold) and more actin tails (3.0- ± 0.8-fold) than control cells (Figure 2F). Similar results were obtained for SEPT9-depleted cells (Figure S2F). Together, these data strongly suggest a reciprocal relationship between septin caging and actin tail formation.

## Cellular Requirements for Septin Cages

We addressed the cellular components required for compartmentalization of *Shigella* by septin cages. The depletion of SEPT2 or SEPT9 eliminated SEPT2-, SEPT9-, and SEPT11-containing cages (Figure 3A). In contrast, and in agreement with the redundancy of SEPT6 group members (Mostowy et al., 2009a; Hanai et al, 2004; Ono et al., 2005), the depletion of SEPT11 did not reduce the number of SEPT2- or SEPT9-containing cages (Figure 3A), suggesting that SEPT11 is dispensable for this process. Treatment of *Shigella*-preinfected cells with cytochalasin D or latrunculin B dramatically reduced the number of *Shigella*-septin cages (4.0- ± 1.1-fold or 3.0- ± 0.3-fold, respectively, Figure 3B; Figure S3A; Movie S7), reinforcing the essential role for actin polymerization in septin cage formation. In contrast, septin cages did not appear to depend on microtubule dynamics since nocodazole, an inhibitor of microtubule polymerization, had no effect (Figure 3B; Figure S3A). Septins have been reported to bind to actin via anillin (Kinoshita et al., 2002) or myosin II (Joo et al., 2007). While critical for cytokinesis (Glotzer, 2001), these interactions during infection have not been investigated. Anillin is confined to the nucleus during interphase (Oegema et al., 2000) and remained in the nucleus throughout infection of interphase cells (Figure S3B). In contrast, myosin II colocalizes with actin and septin filaments in uninfected cells (Joo et al., 2007) and was recruited to septin rings caging *Shigella* (Figure S3C). Phosphorylated myosin light chain (pMLC), a marker of myosin II activation that colocalizes with septin filaments in uninfected cells (Figure S3D), was also detected around caged bacteria (Figures S3E and S3F). Closer investigation of the spatial relationship between pMLC and septin by image deconvolution (Figure 3C; Figure S3E) showed

(C) HeLa cells were transfected with SEPT6-GFP, infected with *S. flexneri* for 4 hr 40 min, fixed for fluorescent light microscopy, and stained with antibodies to N-WASP. The scale bar represents 1 μm. Similar images were obtained for cells transfected with SEPT2 or SEPT9 fluorescent constructs.

(D) HeLa cells were treated with control (CTRL) or N-WASP siRNA. Whole-cell lysates of siRNA-treated cells were immunoblotted for GAPDH or N-WASP to show the efficiency of N-WASP depletion (left). siRNA-treated cells were infected with *S. flexneri* for 4 hr 40 min then fixed and labeled for quantitative microscopy. Graphs (right) represent the mean % ± SEM of *Shigella* inside SEPT2 cages from three independent experiments per treatment. p value, Student's t test. Similar differences were obtained at 1 hr 40 min after infection.

(E) HeLa cells were infected with *S. flexneri* for 1 hr 40 min, 4 hr 40 min, or 6 hr 40 min and fixed and labeled for quantitative microscopy. Data represents the mean % ± SEM of *Shigella* inside SEPT2 cages or forming actin tails from ten (1 hr 40 min), 14 (4 hr 40 min), or three (6 hr 40 min) independent experiments per time point. Similar values were obtained for SEPT9 cages.

(F) HeLa cells were treated with control (CTRL) or SEPT2 siRNA, infected with *S. flexneri* for 4 hr 40 min, and fixed and labeled for quantitative microscopy. Graphs represent the mean % ± SEM of *Shigella* inside SEPT2 cages or forming actin tails from at least three independent experiments per treatment. p values, Student's t test. Similar results were obtained with SEPT9 siRNA (Figure S2F).

See also Figure S2 and Movies S2–S6.

a partial colocalization at the *Shigella*-septin cage. Recruitment of pMLC at the *Shigella*-septin cage was confirmed by CL-SEM and immunogold labeling for pMLC and SEPT6 (Figure 3D). These results clearly showed the arrangement of pMLC and septin filamentous assemblies entrapping bacterium. Together, these observations reveal that activated myosin II is present in cage-like structures around the same subset of bacteria that are also caged by septin.

We treated infected cells harboring *Shigella*-septin cages with blebbistatin, a small molecule known to reduce the affinity of myosin II for actin and inhibit myosin II activity (Straight et al., 2003). As for the pharmacological inhibitors of actin polymerization, inhibition of myosin II function with blebbistatin significantly reduced the number of *Shigella*-septin cages (3.8- ± 0.5-fold, Figure 3B; Figure S3A). These data suggested that *Shigella*-septin caging requires actomyosin activity, a feature well recognized for septin function during cytokinesis (Glotzer, 2001). We thus cotransfected cells with plasmids encoding fluorescent septin and actin constructs, infected these cells with *Shigella*, and examined infected cells treated with blebbistatin by real-time video microscopy. Strikingly, septin cages disassembled and *Shigella* recovered an actin-based motility (Figure 3E; Movie S8), a phenomenon never observed in untreated cells (S.M. and P.C., unpublished data). To further assess the impact of myosin II disruption on the number of motile bacteria, we treated cells with control or myosin II siRNA and compared the number of *Shigella*-septin cages and actin tails in siRNA-treated cells (Figure 3F; Figure S3G). Myosin II-depleted cells had significantly fewer septin cages (3.1- ± 0.5-fold) and more actin tails (2.3- ± 0.4-fold) than control cells, similar to what was observed with septin-depleted cells (Figure 2F; Figure S2F). Together, these data established a role for myosin II in septin caging of intracytosolic *Shigella*.

## Septin Caging Restricts *Shigella* Cell-to-Cell Spread

Actin tail formation is required for *Shigella* intercellular spread. Having demonstrated that the inactivation of septin caging increases the number of *Shigella* with actin tails, we reasoned that septin caging of *Shigella* would restrict its intercellular spreading capacity. The effect of septin depletion on bacterial entry (Mostowy et al., 2009a, 2009b) precludes the use of septin siRNA to quantify bacterial cell-to-cell spread. We thus depleted cells of myosin II by siRNA, infected these cells with *Shigella*, and followed the number of infected cells over time by quantitative microscopy. Strikingly, at later time points, the number of infected cells was significantly increased (2.4- ± 0.8-fold at 4 hr 40 min, Figure 3G). Similar results were obtained by flow cytometry analysis for cells treated with blebbistatin after bacterial internalization (3.4- ± 0.9-fold at 4 hr 40 min, Figure 3H; Figure S3H). These results strongly suggested that myosin II-dependent septin caging restricts *Shigella* cell-to-cell spread. However, an increase in cell-to-cell spread could also reflect the elimination of some other, as yet unidentified, cellular function caused by myosin II inactivation that may facilitate intercellular spread independently of septin caging. To test this hypothesis, we performed cell-to-cell spread experiments using *Listeria*, which also relies on actin tail formation for cell-to-cell spread but for which no efficient septin caging had been observed. Here, blebbistatin treatment did not increase, and even slightly reduced, the number of *Listeria*-infected cells over time (Figure S3I), strongly suggesting that myosin II inactivation does not facilitate cell-to-cell spread and that the inactivation of septin caging is responsible for the increase in *Shigella* cell-to-cell spread. Taken together, these results reveal that septin caging restricts *Shigella* cell-to-cell spread.

## Septin Caging Is Stimulated by Host Factors

We next considered host factors that could control bacterial-septin caging, thereby reducing actin tail formation and cell-to-cell spread. TNF-α is a pleiotropic cytokine that orchestrates a wide range of biological functions, including host defense against pathogens (Locksley et al., 2001), and is prominently induced upon *Shigella*-infection (Perdomo et al., 1994). TNF-α is also known to stimulate actomyosin contractility by increasing the expression of MLC kinase, leading to increased phosphorylation of MLC important for activity of myosin II (Ma et al., 2005; Wang et al., 2005). We therefore tested whether TNF-α could influence septin cage assembly during *Shigella* infection. We first showed by western blot that treatment of uninfected cells with physiologically relevant concentrations of TNF-α increased the association of myosin II to SEPT2 by 3.8- ± 0.3-fold (Figure 4A). Strikingly, cells pretreated with TNF-α and infected with *Shigella* presented a significantly larger number of septin cages (1.8- ± 0.2-fold), often clustered in intracellular microcolonies, and a significantly smaller number of actin tails (2.8- ± 0.3-fold) compared to control cells (Figures 4B and 4C). In addition, the total number of infected cells significantly decreased upon TNF-α treatment at the later time points measured by quantitative microscopy (2.3- ± 0.4-fold at 4 hr 40 min, Figure 4D) and flow cytometry (3.3- ± 0.7-fold at 4 hr 40 min, Figure 4E; Figure S4A), indicative of decreased cell-to-cell spread. To exclude the possibility that the effect of TNF-α on intercellular spread is due to causes other than septin caging, we measured the speed of motile intracytosolic bacteria and showed that it was unaffected by TNF-α (Figure S4B). As a further control, we investigated whether inactivating myosin II can counteract the effects of TNF-α. We treated control and myosin II-depleted cells with TNF-α and infected these cells with *Shigella*. Depletion of myosin II by siRNA prevented the impact of TNF-α on *Shigella* caging and cell-to-cell spread (Figures S4C and S4D). Together, these data highlight that a host factor that regulates SEPT2-myosin II interaction, here TNF-α, can specifically control the entrapment of intracytosolic bacteria and their intercellular spreading capacity.

## Septins Cage Bacteria Targeted to Autophagy

Interestingly, *Shigella*-induced actin polymerization and autophagosome formation have both been shown to depend on IcsA (Ogawa et al., 2005). As septin caging also depends on IcsA, we reasoned that bacteria in septin cages may be compartmentalized for autophagy. In line with this hypothesis, we observed ubiquitylated proteins around *Shigella* present in septin cages (Figure S5A) and pharmacological inhibitors of the proteasome did not affect *Shigella*-septin cage formation (Figure S5B). p62 (SQSTM1), a protein recently associated with intracytosolic *Shigella* (Dupont et al., 2009) that binds ubiquitin and Atg8 (LC3) (Pankiv et al., 2007), the marker widely used to define autophagosomes (Mizushima et al., 2010), was recruited

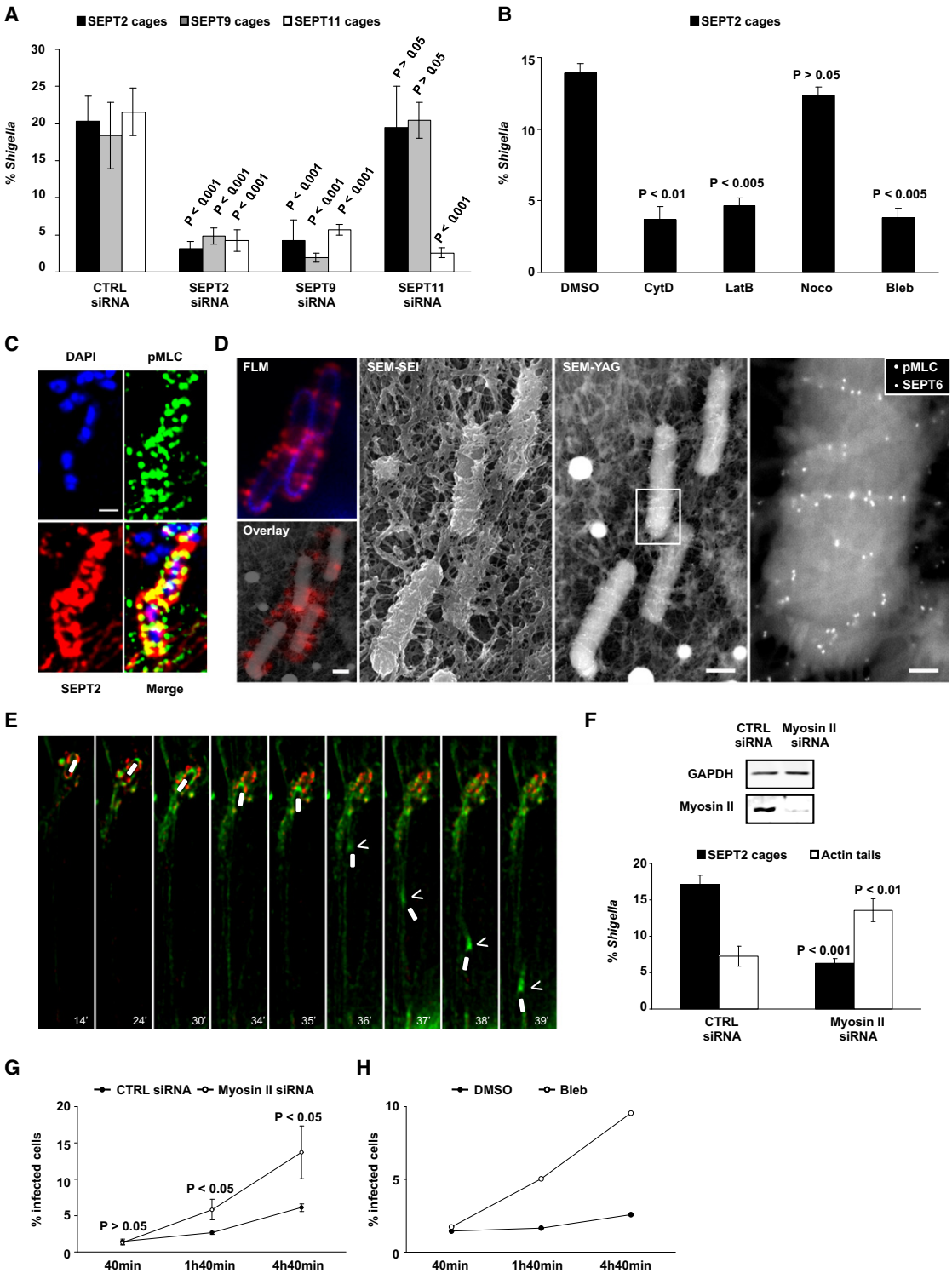


**Figure 3. Cellular Requirements for *Shigella*-Septin Cage Formation**

(A) HeLa cells were treated with control (CTRL), SEPT2, SEPT9, or SEPT11 siRNA, infected with *S. flexneri* for 4 hr 40 min, and fixed and labeled for quantitative microscopy. Graphs represent the mean % ± SEM of *Shigella* inside SEPT2, SEPT9, or SEPT11 cages from at least three independent experiments per treatment. p values were obtained from comparison to CTRL cells, Student's t test.

(B) HeLa cells were infected with *S. flexneri*, treated with DMSO, cytochalasin D (CytD), latrunculin B (LatB), nocodazole (Noco), or blebbistatin (Bleb) and after 4 hr 40 min were fixed and labeled for quantitative microscopy. Graphs represent the mean % ± SEM of *Shigella* inside SEPT2 cages from two independent experiments per treatment. p values, Student's t test. Similar results were obtained for SEPT9 or SEPT11 cages (Figure S3A).

to *Shigella*-septin cages (Figure 5A). Moreover, *Shigella*-septin cages also colocalized with Atg8 (Figure 5B). Together, these data suggested that *Shigella* compartmentalized by septin cages are also targeted to autophagy.

*Shigella* can escape autophagy by a mechanism dependent on IcsB (Ogawa et al., 2005; Travassos et al., 2010). To further validate that bacteria in septin cages are targeted to autophagy, we analyzed the behavior of an IcsB mutant. We observed that, as for wild-type bacteria, ubiquitylated proteins were concentrated around bacteria in septin cages (Figure S5C). Moreover, *Shigella* lacking IcsB was compartmentalized in septin cages more efficiently than the wild-type strain (2.4- ± 0.2-fold, Figure 5C), suggesting that autophagy and septin cage assembly contribute to the same process.

We thus used siRNAs to deplete cells of the autophagy proteins p62, Atg5, Atg6 (Beclin1, a protein crucial for autophagy initiation), or Atg7 (the activating enzyme for Atg8 conjugation) and evaluated septin caging in these siRNA-treated cells (Figure 5D). In each case, septin caging was significantly reduced (3.6- ± 0.3-fold, 2.6- ± 0.3-fold, 2.8- ± 0.5-fold, or 2.1- ± 0.3-fold, respectively), demonstrating that septin cage assembly is more efficient once the process of autophagy has been initiated.

To address the impact of septin depletion on cellular autophagic activity, we used an established autophagosome turnover assay that examines the steady state levels of p62 and Atg8-II in the presence and absence of bafilomycin (an inhibitor of autophagosome-lysosome fusion) (Mizushima et al., 2010). Accordingly, the differences in the amount of p62 and Atg8-II between samples represent the amount that is delivered to lysosomes for degradation (i.e., autophagic flux). Strikingly, levels of p62 and Atg8-II were significantly reduced in cells depleted for SEPT2 or SEPT9 in the presence (p62 by 3.1- ± 0.7-fold or 2.6- ± 0.4-fold, respectively, and Atg8-II by 2.2- ± 0.6-fold or 1.8- ± 0.6-fold, respectively) and absence (p62 by 2.0- ± 0.4-fold or 1.7- ± 0.0-fold, respectively, and Atg8-II by 3.1- ± 0.6-fold or 1.8- ± 0.2-fold, respectively) of bafilomycin (Figure 5E). To confirm that septin depletion results in a reduction of autophagic activity, we first observed that 86% ± 4% of *Shigella* recruiting p62 were also in septin cages (mean ± SEM from n = 4 experiments). We then used siRNA to deplete cells of SEPT2 or SEPT9 and evaluated p62 recruitment to *Shigella* in these siRNA-treated cells (Figure 5F). In both cases, p62 recruitment was significantly reduced (4.5- ± 0.4-fold or 4.2- ± 0.7-fold, respectively). These results suggest a general role for septins in autophagic activity and, together with the concept of septin caging during bacterial infection, provide a so far unsuspected view on how the cytosketon is involved in autophagy.

## DISCUSSION

A well-studied strategy employed by different pathogens, including *Listeria* and *Shigella*, for efficient infection is the subversion of the actin cytoskeleton to move intra- and intercellularly (Gouin et al., 2005). The study of actin-based motility is one of the best examples of how understanding a bacterial-induced process can yield insight into basic cellular processes. *Listeria* and ActA have been particularly instrumental in the discovery of the role of Arp2/3 (Welch et al., 1997), and work performed since then has identified the other proteins essential for actin-based motility in vitro (Loisel et al., 1999). How the many other actin-binding proteins regulate this process in cellular environments is considerably less defined (Van Troys et al., 2008), yet this knowledge is necessary for a complete understanding of infectious processes. Our data examining actin tails in septin-depleted cells suggest that septin recruitment to already motile bacteria does not affect the speed of movement (Figures 1D and 1E), although a possibility exists that septin recruitment may serve a role during bacterial motility in particular conditions. In this study we focused our analysis on septin recruitment to non-motile bacteria.

We have shown that *Shigella*-infected host cells can prevent actin-based motility by compartmentalizing bacteria inside septin cages, a process that relies on actin polymerization and autophagosome formation, according to the scenario proposed in Figure 6A: *Shigella* escape from the phagocytic vacuole into the cytosol, where they start polymerizing actin via IcsA. Concurrently, *Shigella* IcsA can induce autophagy by binding to the autophagy protein Atg5 (Ogawa et al., 2005). IcsA-mediated

(C) HeLa cells were infected with *S. flexneri* for 4 hr 40 min, fixed for fluorescent light microscopy, and stained with antibodies to pMLC and SEPT2. To further resolve the location of pMLC at *Shigella*-septin cages, deconvolution was performed (here and Figure S3E). The scale bar represents 1 μm. Similar images were obtained labeling for SEPT9 (Figure S3F).

(D) HeLa cells were transfected with SEPT6-GFP, infected with *S. flexneri* for 4 hr 40 min, and processed for CL-SEM. SEPT6 is shown in red and bacteria in blue. Septin cages identified by fluorescent light microscopy (FLM) were processed for SEM (overlay; scale bar represents 0.5 μm). The SEM-SEI image shows the morphology of septin cages, and the SEM-YAG image (scale bar represents 0.5 μm) shows the immunogold labeling of endogenous pMLC (20 nm particles) and GFP (i.e., SEPT6, 10 nm particles). The right-most image (scale bar represents 0.1 μm) is enlarged from the boxed region in the SEM-YAG image.

(E) HeLa cells were transfected with actin-CFP and SEPT9-tdTomato, infected with *S. flexneri* for 2 hr, and prepared for real-time video microscopy. Image series were collected every 60 s for 40 min, where after the first 5 min cells were treated with blebbistatin. Actin is shown in green and SEPT9 in red. White bodies mark the bacterium, white arrowheads point to the actin tail, and time/frame is in the lower right corner. The entire image sequence can be viewed as Movie S8.

(F) HeLa cells were treated with control (CTRL) or myosin II siRNA. Whole-cell lysates of siRNA-treated cells were immunoblotted for GAPDH or myosin II to show the efficiency of myosin II depletion (top). siRNA-treated cells were infected with *S. flexneri* for 4 hr 40 min and fixed and labeled for quantitative microscopy. Graphs (bottom) represent the mean % ± SEM of *Shigella* inside SEPT2 cages from five independent experiments per treatment. p values, Student's t test. Similar results were obtained for SEPT9 cages (Figure S3G).

(G) HeLa cells were treated with control (CTRL) or myosin II siRNA, infected with *S. flexneri* for 40 min, 1 hr 40 min, or 4 hr 40 min and fixed and labeled for quantitative microscopy. Values represent the mean % ± SEM of infected cells from at least three independent experiments per siRNA treatment per time point. p values, Student's t test.

(H) Caco-2 cells were infected with *S. flexneri*-GFP for 40 min, treated with DMSO or blebbistatin (Bleb) for 1 hr, 4 hr, or 6 hr, and fixed for flow cytometry. Values are the % of cells that were infected. One representative time course comparing DMSO- and Bleb-treated cells of four is shown, and the others are shown as Figure S3H. Differences were continued at 6 hr 40 min.

See also Figure S3 and Movies S7 and S8.

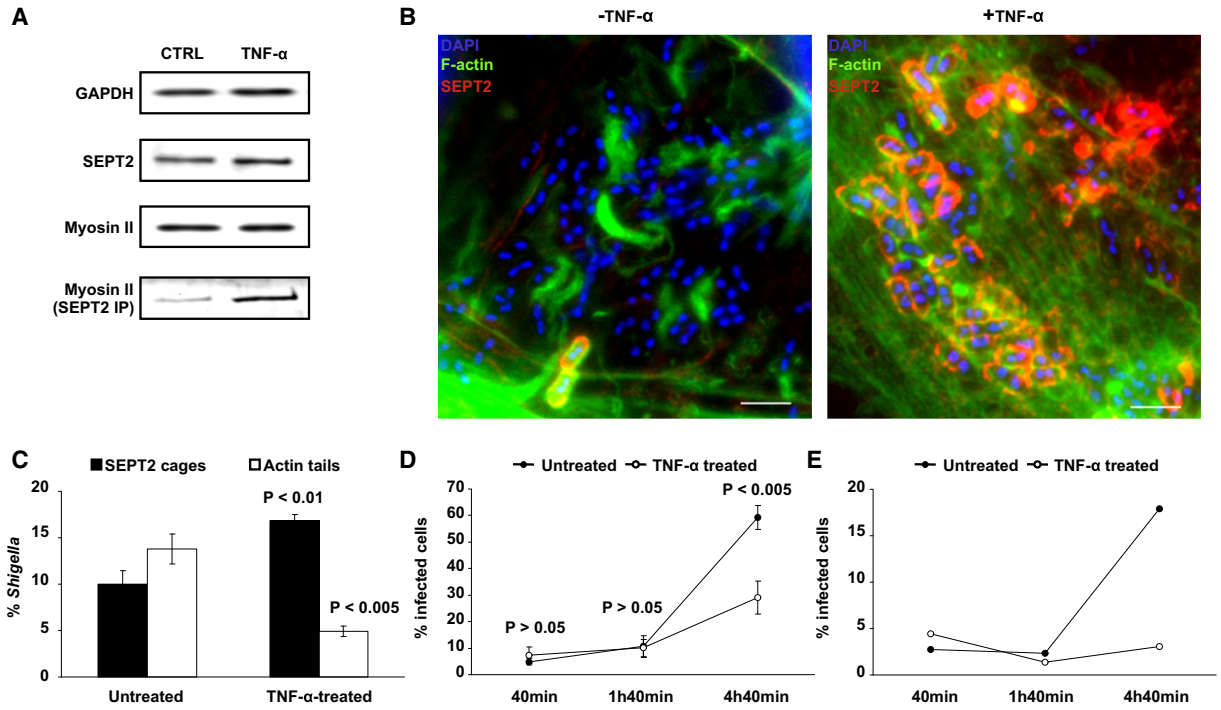


**Figure 4. TNF-α Increases Septin Cage Formation and Inhibits *Shigella* Cell-to-Cell Spread**

(A) Immunoprecipitation experiments were performed with antibodies to SEPT2 and lysates from untreated or TNF-α-treated Caco-2 cells. Cell lysates prior to the immunoprecipitation step and immunoprecipitated protein were revealed using antibodies to GAPDH, SEPT2, or myosin II. Representative blots from three independent experiments are shown.

(B) Untreated or TNF-α-treated Caco-2 cells were infected with *S. flexneri* for 4 hr 40 min, fixed for fluorescent light microscopy, and stained with phalloidin and antibodies to SEPT2. Scale bars represent 5 μm.

(C) Untreated or TNF-α-treated Caco-2 cells were infected with *S. flexneri* for 4 hr 40 min and fixed and labeled for quantitative microscopy. Graphs represent the mean % ± SEM of *Shigella* inside SEPT2 cages or forming actin tails from three independent experiments per treatment. p values, Student's t test.

(D) Untreated or TNF-α-treated Caco-2 cells were infected with *S. flexneri* for 40 min, 1 hr 40 min, or 4 hr 40 min and fixed and labeled for quantitative microscopy. Values represent the mean % ± SEM of cells that were infected from at least three independent experiments per treatment per time point. p values, Student's t test.

(E) Untreated or TNF-α-treated Caco-2 cells were infected with *S. flexneri*-GFP for 40 min, 1 hr 40 min, 4 hr 40 min, or 6 hr 40 min and fixed for flow cytometry. Values are the % of cells that were infected. One representative time course comparing untreated and TNF-α-treated cells of five is shown, and the others are shown as Figure S4A. Differences were continued at 6 hr 40 min.

See also Figure S4.

actin polymerization and autophagosome marker recruitment can lead to septin cage assembly and thus productive autophagy. However, when Atg5-IcsA binding is competitively inhibited by *Shigella* IcsB as shown previously (Ogawa et al., 2005), autophagosome initiation is avoided, septin cages cannot assemble efficiently, and *Shigella* dissemination by actin-based motility proceeds, ultimately resulting in cell-to-cell spread. A number of components may direct *Shigella* toward septin caging or toward actin tail formation, and host factors induced upon infection are likely to be critical for containing bacterial dissemination in vivo. Such a factor is TNF-α, a cytokine well known to be induced upon *Shigella*-infection (Perdomo et al., 1994) and shown here to stimulate septin cage assembly (Figures 4B and 4C).

In the case of *Listeria*, no efficient septin caging had been observed in the conditions tested here (Figure S2A). *Listeria* has been reported to avoid autophagy by expressing ActA, and ActA mutants are efficiently targeted to autophagy (Yoshikawa et al., 2009). Considering that in the case of *Shigella* septin cage assembly is both actin dependent and autophagy connected, we propose that *Listeria*, via its surface expression of ActA, evades both septin caging and autophagy (Figure 6B). It is clear that in-depth investigation of infection by other bacteria that polymerize actin will help to precisely describe the coordination between septin caging and autophagy. In this respect, preliminary data show that *Rickettsia conorii*, which is similar to *Listeria* in that it expresses a bacterial effector (i.e., RickA) to activate Arp2/3 for actin tail polymerization (Gouin et al., 2004), is not efficiently compartmentalized by septin cages (data not shown). In contrast, *Mycobacterium marinum*, which is similar to *Shigella* in that it recruits WASP-family proteins for actin tail polymerization (Stamm et al., 2003), is observed in septin cage-like structures (Figure S6A).

What is the fate of bacteria compartmentalized by septin cages? Autophagy, a process in which the cell sequesters cytosolic constituents in a double membrane vesicle and delivers them to the lysosome for degradation, has been recognized as a crucial defense mechanism against *Shigella* (Dupont

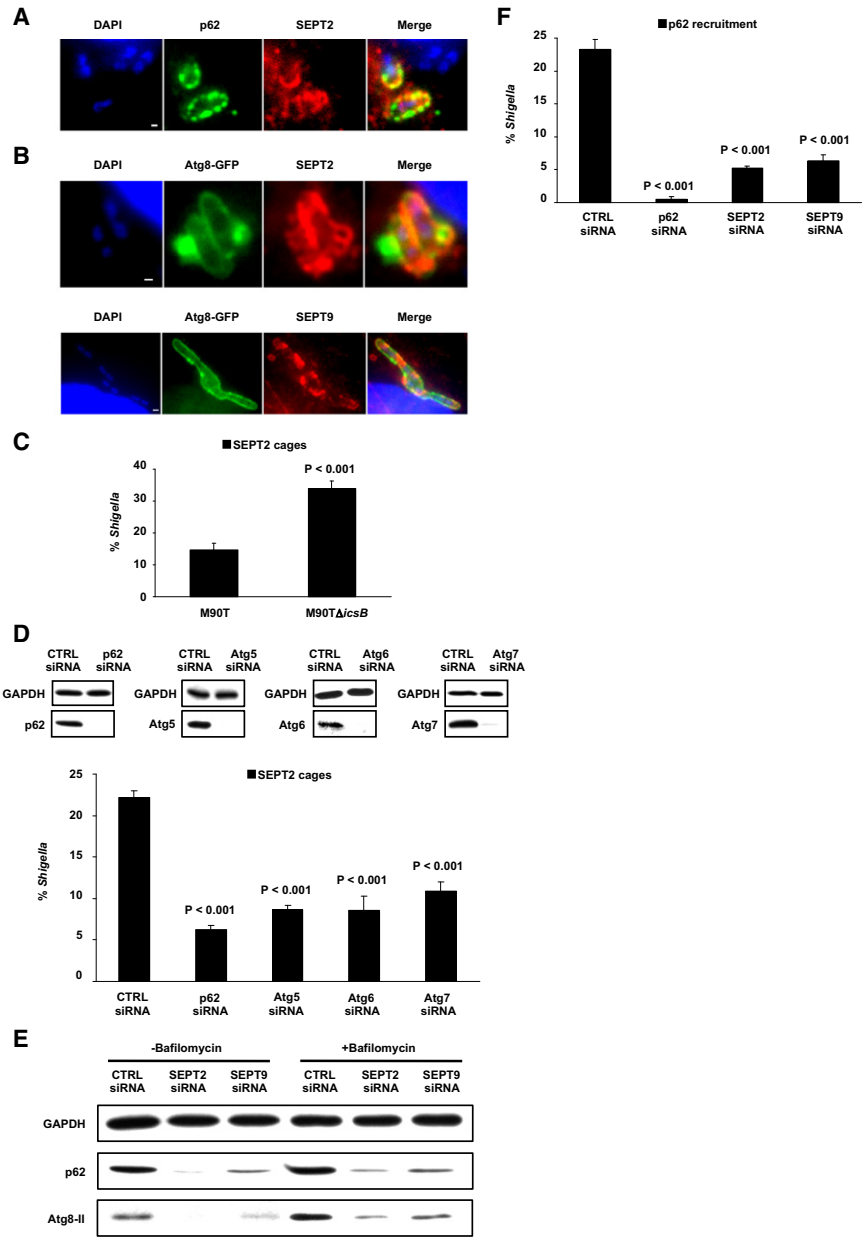


**Figure 5. Septin Cages Entrap *Shigella* Targeted to Autophagy**

(A) HeLa cells were infected with *S. flexneri* for 4 hr 40 min, fixed for fluorescent light microscopy, and stained with antibodies to SEPT2 and p62. The scale bar represents 1 μm. Similar images were obtained labeling for SEPT9.

(B) HeLa cells were transfected with Atg8-GFP, infected with *S. flexneri* for 4 hr 40 min, fixed for fluorescent light microscopy, and stained with antibodies to SEPT2 or SEPT9. Scale bars represent 1 μm (top) and 2 μm (bottom). Similar localization of SEPT9-tdTomato or SEPT9-CFP at Atg8-GFP-positive *Shigella* was observed in real-time.

(C) HeLa cells were infected with *S. flexneri* for 4 hr 40 min and fixed and labeled for quantitative microscopy. Graphs represent the mean % ± SEM of *Shigella* M90T or M90TΔ*icsB* found inside SEPT2 cages from five independent experiments per strain. p values, Student's t test.

(D) HeLa cells were treated with control (CTRL), p62, Atg5, Atg6, or Atg7 siRNA. Whole-cell lysates of siRNA-treated cells were immunoblotted for GAPDH, p62, Atg5, Atg6, or Atg7 to show the efficiency of siRNA depletion (top). siRNA-treated cells were infected with *S. flexneri* for 4 hr 40 min and fixed and labeled for quantitative microscopy. Graphs (bottom) represent the mean % ± SEM of *Shigella* inside SEPT2 cages from at least three independent experiments per treatment. p values, Student's t test.

(E) HeLa cells were treated with control (CTRL), SEPT2, or SEPT9 siRNA, treated or not with bafilomycin, and immunobloted for GAPDH, p62, or Atg8. Representative blots from three independent experiments are shown. Similar differences in the levels of autophagic markers were observed for siRNA-treated cells infected with *Shigella* for 4 hr 40 min in the presence and absence of bafilomycin.

(F) HeLa cells were treated with control (CTRL), p62, SEPT2, or SEPT9 siRNA, infected with *S. flexneri* for 4 hr 40 min, and fixed and labeled for quantitative microscopy. Graphs represent the mean % ± SEM of *Shigella* with p62 recruitment from at least two independent experiments per treatment.

See also Figure S5.

et al., 2009; Ogawa et al., 2005; Travassos et al., 2010. We have shown that septins are recruited with autophagy proteins to intracytosolic *Shigella* and that septin cages require autophagosome initiation. There seems to be an interdependence between the two evolutionarily conserved processes of septin assembly and autophagy. We propose that septin cages assemble after autophagic recognition and that productive autophagy benefits from the entrapment of actin-polymerizing bacteria by septin cages. It is likely that other autophagic activities also benefit from septin assembly, and we have observed that the levels of autophagy critical components are strikingly reduced upon septin depletion (Figures 5E and 5F). Relatively little is known about the roles of the cytoskeleton in autophagy. It will thus be of great interest to further study the link between actin polymerization, septin cages, autophagy, and pathogen dissemination.

## EXPERIMENTAL PROCEDURES

### Bacterial Strains and Cell Culture

Please refer to the Supplemental Experimental Procedures.

### Antibodies

Rabbit polyclonal antibodies used were anti-SEPT9 (R69) (Pizarro-Cerdá et al., 2002), anti-SEPT11 (Tada et al., 2007), anti-NWASP (Bierne et al., 2005), anti-anillin (Oegema et al., 2000), anti-non-muscle myosin IIA (Biomedical Technologies, Ref#BT-567 or Sigma, Ref#M8064), anti-Atg5 (Novus Biologicals, Ref#NB110-53818), anti-Atg7 (Sigma, Ref#A2856), and anti-Atg8 (Novus Biologicals, Ref#NB100-2331). Polyclonal antipeptide antibodies that recognize

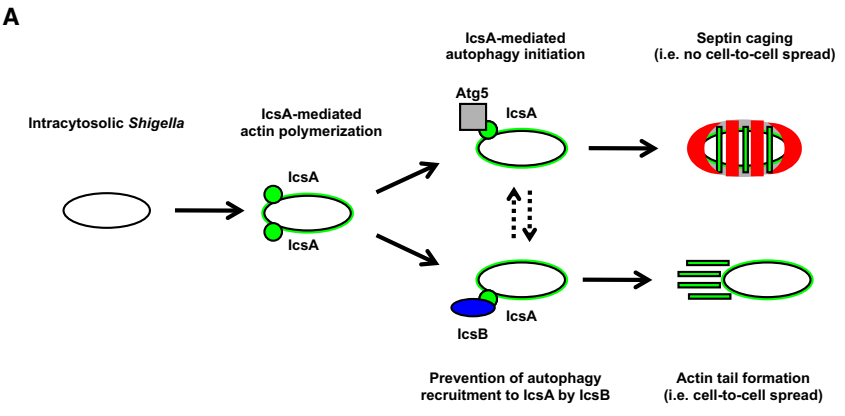


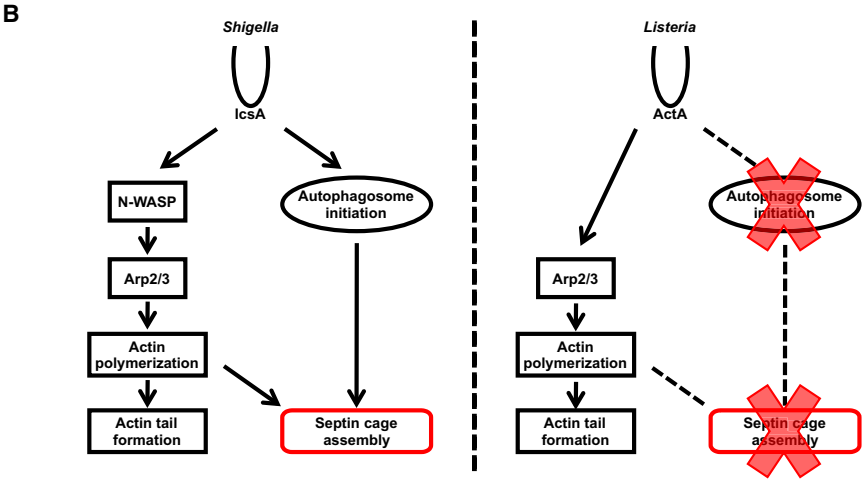


**Figure 6. Septin Caging of Intracytosolic Bacteria**

(A) Proposed circumstance of *Shigella*-septin caging versus actin tail formation. Depending on the availability of IcsA, *Shigella* will be compartmentalized in septin cages or spread cell-to-cell via actin-based motility.

(B) Model depicting why *Shigella* efficiently recruits septin cages but *Listeria* does not. *Shigella* IcsA-mediated actin polymerization and autophagosome recruitment together are both essential for intracytosolic septin cage assembly. Alternatively, *Listeria* avoids autophagy by expressing ActA. Considering that septin assembly requires autophagosome formation, *Listeria* also avoids septin cage formation.

See also Figure S6.

SEPT2 (Xie et al., 1999) or SEPT7 (Tada et al., 2007) were also obtained as described in (Pizarro-Cerdá et al., 2002). Mouse monoclonal antibodies used were anti-GAPDH (AbCam, Ref#6C5), anti-phospho-MLC2 (Ser 19, Cell Signaling Ref#3675), FK2 (Enzo Life Sciences, Ref#PW8810), FK1 (Enzo Life Sciences, Ref#PW8805), anti-p62 lck ligand (BD Biosciences, Ref#610832), and anti-Beclin (BD Biosciences, Ref#612112). Secondary antibodies used were Cy5- (Jackson ImmunoResearch Laboratories) and Alexa 488- or 546-conjugated goat anti-rabbit or goat anti-mouse (Molecular Probes). F-actin was labeled with Alexa 488-, 546-, or 647-phalloidin (Molecular Probes).

For immunoblotting, total cellular extracts were blotted with the above-mentioned antibodies, followed by peroxidase-conjugated goat anti-mouse or anti-rabbit antibodies (Biosys Laboratories). GAPDH was used throughout as a loading control. Proteins were run on 8%, 10%, or 14% acrylamide gels.

### Immunoprecipitation Studies

Cells were lysed in Igepal buffer (20 mM Tris [pH 8.0], 1% [v/v] Igepal CA-630 [Sigma], 150 mM NaCl, 10% [v/v] glycerol, and protease inhibitors cocktail). Myosin II was immunoprecipitated from 800 μg of the total protein extracts by addition 1 μg of anti-SEPT2 antibody and 40 μl of a 50% slurry suspension of Protein-A-Sepharose beads (Amersham Biosciences Biotech). Samples were analyzed by SDS-polyacrylamide gel electrophoresis (SDS–PAGE) and immunoblotted with anti-myosin II antibody. HRP-conjugated goat anti-rabbit secondary antibodies were subsequently used. Protein input was evaluated by probing blots of cell lysates prior to the immunoprecipitation step using antibodies specific to GAPDH, SEPT2, or myosin II. The relative amount of myosin II protein after SEPT2 immunoprecipitation was quantified with GeneTools (SynGene).

### Infections and Microscopy

HeLa or Caco-2 cells (1–1.5 × $10^5$) were plated on glass coverslips in 6-well plates (Techno Plastic Products) and used for experiments 48 hr later. Cells on coverslips were fixed 15 min in 4% paraformaldehyde (PFA) and were then washed with 1 × PBS and processed for immunofluorescence (IF). After 10 min of incubation in 50 mM ammonium chloride, cells were permeabilized 4 min with 0.1% Triton X-100 and then incubated in 1 × PBS. Incubation with primary or secondary antibodies was performed in 1 × PBS. Vectashield hard set mounting medium with DAPI (Vector Laboratories) or mounting medium for IF (Interchim) was used.

*Listeria* was added to host cells at a multiplicity of infection (MOI) of 50 (for flow cytometry analysis) or 100. Bacteria and cells were centrifuged at 1000 g for 1 min at 21°C and were then incubated at 37°C and 10% $CO_2$ for 40 min (for flow cytometry analysis) or 1 hr, washed with MEM, and incubated with fresh gentamicin-containing complete media (10 μg/ml) for an additional 1, 2, 4, or 6 hr, after which they were washed with 1 × PBS and fixed and processed for IF. *Shigella* was added to cells at an MOI of 100 (for quantification analyses) or 400 μl of growth ($OD_{600nm}$ = 0.6) was diluted in MEM and directly added to cells (for imaging analyses). Bacteria and cells were centrifuged at 700 g for 10 min at 21°C and were then placed at 37°C and 10% $CO_2$ for 30 min, washed with MEM, and incubated with fresh gentamicin-containing complete media (50 μg/ml) for 1, 2, 4, or 6 hr, after which they were washed with 1 × PBS and fixed and processed for IF. For infection of cells with *M. marinum*, 2 × $10^5$ RAW macrophages were plated onto glass coverslips in 6-well plates and used for experiments 48 hr later. *M. marinum* was washed twice in 1 × PBS and passaged through a 26 gauge needle. Bacteria were added to cells in media without FCS at an MOI of 10. Bacteria and cells were centrifuged at 700 g for 5 min at 21°C then placed for 2 hr at 32°C and 5% $CO_2$. Infected cells were then washed with 1 × PBS and incubated with 200 μg/ml amikacin for 2 hr at 32°C and 5% $CO_2$. After this time, macrophages were washed with 1 × PBS and incubated in complete media at 32°C and 5% $CO_2$ for 20 or 44 hr. After a total of 24 or 48 hr, infected cells were washed with 1 × PBS and fixed and processed for IF.

Images were acquired on a fluorescence inverted microscope Axiovert 200M (Carl Zeiss MicroImaging) equipped with a cooled digital charge-coupled device camera (Cool $SNAP_{HQ}$, Photometrics) driven by Metamorph Imaging System software (Universal Imaging). For 3D representation, quantitative microscopy (i.e., counting of septin cages and actin tails) was performed with a Z stack image series of infected cells, counting 250–1000 bacteria per experiment. Confocal images were acquired with a Leica TCS SP5 laser-scanning microscope (Leica microsystems) or a spinning-disk confocal

microscope system (Andor technology) on an Axiovert 200M microscope equipped with an iXon+ DV885 EMCCD camera (Andor technology). Images were processed with ImageJ (http://rsb.info.nih.gov/ij/). 3D reconstruction was performed with Imaris analysis software (http://www.bitplane.com/). Deconvolution was performed with Huygens deconvolution software (Scientific Volume Imaging). For measurement of the velocity of motile bacteria, image series were collected every 10 s for 1–40 min. Individual bacterium with actin tails were followed for 1–10 min, and velocities were calculated with the Manual Tracking plugin for ImageJ.

Real-time IF microscopy was performed with actin-YFP (BUG 2016), actin-CFP (BUG 2155), SEPT2-YFP (BUG 2444), SEPT6-GFP (BUG 2445), SEPT9-CFP (BUG 2309), SEPT9-tdTomato (BUG 2310), or Atg8-GFP (Dupont et al., 2009). HeLa cells were transfected with jetPEI (PolyPlus Transfection). Once placed on the microscope stage at 37°C, image series of infected cells were collected every 10–60 s for 5–90 min depending on the experiment.

For experimental procedures involving STORM, CL-SEM, and FRAP, please refer to the Supplemental Experimental Procedures.

### siRNA, Pharmacological Inhibitors, and TNF-α Treatment

HeLa cells ($0.8 \times 10^5$) were plated in 6-well plates and transfected the following day with oligofectamine (Invitrogen). Control siRNA (Cat#AM4635) and predesigned siRNA for SEPT2 (ID#14709), SEPT9 (ID#18228), Myosin II (MYH9) (ID#S222), N-WASP (WASL) (ID#137397), or Atg5 (ID#s18160) were all from Ambion. siRNA sequences for p62, Atg6, and Atg7 were taken from (Pohl and Jentsch, 2009). Cells were tested 72 hr after siRNA transfection.

For experiments involving pharmacological inhibitors, HeLa cells were infected and treated for 30 min prior to fixation with DMSO, cytochalasin D (5 μM), latrunculin B (5 μM), or nocodazole (5 μM) or 60 min prior to fixation with blebbistatin (50 μM). Drugs were suspended in DMSO and handled as suggested by the manufacturer (Sigma). For inhibition of the proteasome, cells were treated after 40 min of infection with 20 μM of MG-132 (Calbiochem) or Lactacystin (Sigma) for 4 hr. For monitoring of autophagic flux, cells were treated with bafilomycin A1 (Sigma, B1793) for 12 hr or 4 hr during infection (160 nM). For experiments involving TNF-α (R&D systems, Cat#210-TA), cells were treated with 20 ng/ml TNF-α for 20 hr. Treatment was continued throughout infection.

### Flow Cytometry

Treated and infected Caco-2 cells were washed in 1 × PBS, detached with 0.05% EDTA-Trypsin, and permeabilized/fixed with the BD Cytofix/Cytoperm Fixation/Permeabilization kit (BD Biosciences Cat#554714). Samples were analyzed with a FACSCalibur instrument (BD Biosciences). Dead cells were excluded on the basis of forward and side scatter, and a minimum of 20,000 events were acquired per sample. Results were analyzed with FlowJo software (http://www.flowjo.com/).

## SUPPLEMENTAL INFORMATION

Supplemental Information includes Supplemental Experimental Procedures, six figures, and eight movies and can be found with this article online at doi:10.1016/j.chom.2010.10.009.

## ACKNOWLEDGMENTS

We thank members of the J. Enninga and P. Sansonetti laboratories for *Shigella* tools. We thank E. Spiliotis for fluorescent septin constructs, L. Ramakrishnan, T. Soldati, and E. Colucci-Guyon for *M. marinum* strains, C. Machu and G. Azar for image analysis, and O. Disson, G. Nikitas, C. Aubry, D. Ribet, J. Pizarro-Cerdá, M.A. Nahori, O. Dussurget, and V. Villiers for different infections. S.M. is supported by a long-term fellowship from the Canadian Institutes of Health Research. P.C. is an international research scholar from the Howard Hughes Medical Institute and recipient of a European Research Council Advanced Grant Award (233348).

Received: August 31, 2010
Revised: September 23, 2010
Accepted: October 7, 2010
Published: November 17, 2010

## REFERENCES

Bierne, H., Miki, H., Innocenti, M., Scita, G., Gertler, F.B., Takenawa, T., and Cossart, P. (2005). WASP-related proteins, Abi1 and Ena/VASP are required for *Listeria* invasion induced by the Met receptor. J. Cell Sci. *118*, 1537–1547.

Byers, B., and Goetsch, L. (1976). A highly ordered ring of membrane-associated filaments in budding yeast. J. Cell Biol. *69*, 717–721.

Deretic, V., and Levine, B. (2009). Autophagy, immunity, and microbial adaptations. Cell Host Microbe *5*, 527–549.

Dupont, N., Lacas-Gervais, S., Bertout, J., Paz, I., Freche, B., Van Nhieu, G.T., van der Goot, F.G., Sansonetti, P.J., and Lafont, F. (2009). *Shigella* phagocytic vacuolar membrane remnants participate in the cellular response to pathogen invasion and are regulated by autophagy. Cell Host Microbe *6*, 137–149.

Glotzer, M. (2001). Animal cell cytokinesis. Annu. Rev. Cell Dev. Biol. *17*, 351–386.

Gouin, E., Egile, C., Dehoux, P., Villiers, V., Adams, J., Gertler, F., Li, R., and Cossart, P. (2004). The RickA protein of *Rickettsia conorii* activates the Arp2/3 complex. Nature *427*, 457–461.

Gouin, E., Welch, M.D., and Cossart, P. (2005). Actin-based motility of intracellular pathogens. Curr. Opin. Microbiol. *8*, 35–45.

Hall, P.A., and Russell, S.E. (2004). The pathobiology of the septin gene family. J. Pathol. *204*, 489–505.

Hall, P.A., Russell, H.S.E., and Pringle, J.R. (2009). The Septins (Chichester, UK: Wiley InterScience).

Hanai, N., Nagata, K., Kawajiri, A., Shiromizu, T., Saitoh, N., Hasegawa, Y., Murakami, S., and Inagaki, M. (2004). Biochemical and cell biological characterization of a mammalian septin, Sept11. FEBS Lett. *568*, 83–88.

Hartwell, L.H. (1971). Genetic control of the cell division cycle in yeast. IV. Genes controlling bud emergence and cytokinesis. Exp. Cell Res. *69*, 265–276.

Huang, Y.-W., Yan, M., Collins, R.F., Diciccio, J.E., Grinstein, S., and Trimble, W.S. (2008). Mammalian septins are required for phagosome formation. Mol. Biol. Cell *19*, 1717–1726.

Ihara, M., Yamasaki, N., Hagiwara, A., Tanigaki, A., Kitano, A., Hikawa, R., Tomimoto, H., Noda, M., Takanashi, M., Mori, H., et al. (2007). Sept4, a component of presynaptic scaffold and Lewy bodies, is required for the suppression of α-synuclein neurotoxicity. Neuron *53*, 519–533.

Joo, E., Surka, M.C., and Trimble, W.S. (2007). Mammalian SEPT2 is required for scaffolding nonmuscle myosin II and its kinases. Dev. Cell *13*, 677–690.

Kinoshita, M. (2006). Diversity of septin scaffolds. Curr. Opin. Cell Biol. *18*, 54–60.

Kinoshita, M., Field, C.M., Coughlin, M.L., Straight, A.F., and Mitchison, T.J. (2002). Self- and actin-templated assembly of Mammalian septins. Dev. Cell *3*, 791–802.

Kuhlenbäumer, G., Hannibal, M.C., Nelis, E., Schirmacher, A., Verpoorten, N., Meuleman, J., Watts, G.D.J., De Vriendt, E., Young, P., Stögbauer, F., et al. (2005). Mutations in SEPT9 cause hereditary neuralgic amyotrophy. Nat. Genet. *37*, 1044–1046.

Levine, B., and Deretic, V. (2007). Unveiling the roles of autophagy in innate and adaptive immunity. Nat. Rev. Immunol. *7*, 767–777.

Locksley, R.M., Killeen, N., and Lenardo, M.J. (2001). The TNF and TNF receptor superfamilies: integrating mammalian biology. Cell *104*, 487–501.

Loisel, T.P., Boujemaa, R., Pantaloni, D., and Carlier, M.-F. (1999). Reconstitution of actin-based motility of *Listeria* and *Shigella* using pure proteins. Nature *401*, 613–616.

Ma, T.Y., Boivin, M.A., Ye, D., Pedram, A., and Said, H.M. (2005). Mechanism of TNF-α modulation of Caco-2 intestinal epithelial tight junction barrier: role of myosin light-chain kinase protein expression. Am. J. Physiol. Gastrointest. Liver Physiol. *288*, G422–G430.

Mizushima, N., Yoshimori, T., and Levine, B. (2010). Methods in mammalian autophagy research. Cell *140*, 313–326.

Mostowy, S., Danckaert, A., Tham, T.N., Machu, C., Guadagnini, S., Pizarro-Cerdá, J., and Cossart, P. (2009a). Septin 11 restricts InlB-mediated invasion by *Listeria*. J. Biol. Chem. *284*, 11613–11621.

Mostowy, S., Nam Tham, T., Danckaert, A., Guadagnini, S., Boisson-Dupuis, S., Pizarro-Cerdá, J., and Cossart, P. (2009b). Septins regulate bacterial entry into host cells. PLoS ONE *4*, e4196.

Münz, C. (2009). Enhancing immunity through autophagy. Annu. Rev. Immunol. *27*, 423–449.

Oegema, K., Savoian, M.S., Mitchison, T.J., and Field, C.M. (2000). Functional analysis of a human homologue of the *Drosophila* actin binding protein anillin suggests a role in cytokinesis. J. Cell Biol. *150*, 539–552.

Ogawa, M., Yoshimori, T., Suzuki, T., Sagara, H., Mizushima, N., and Sasakawa, C. (2005). Escape of intracellular *Shigella* from autophagy. Science *307*, 727–731.

Ono, R., Ihara, M., Nakajima, H., Ozaki, K., Kataoka-Fujiwara, Y., Taki, T., Nagata, K.-i., Inagaki, M., Yoshida, N., Kitamura, T., et al. (2005). Disruption of Sept6, a fusion partner gene of MLL, does not affect ontogeny, leukemogenesis induced by MLL-SEPT6, or phenotype induced by the loss of Sept4. Mol. Cell. Biol. *25*, 10965–10978.

Pankiv, S., Clausen, T.H., Lamark, T., Brech, A., Bruun, J.-A., Outzen, H., Øvervatn, A., Bjørkøy, G., and Johansen, T. (2007). p62/SQSTM1 binds directly to Atg8/LC3 to facilitate degradation of ubiquitinated protein aggregates by autophagy. J. Biol. Chem. *282*, 24131–24145.

Perdomo, O.J., Cavaillon, J.M., Huerre, M., Ohayon, H., Gounon, P., and Sansonetti, P.J. (1994). Acute inflammation causes epithelial invasion and mucosal destruction in experimental shigellosis. J. Exp. Med. *180*, 1307–1319.

Pizarro-Cerdá, J., Jonquières, R., Gouin, E., Vandekerckhove, J., Garin, J., and Cossart, P. (2002). Distinct protein patterns associated with *Listeria monocytogenes* InlA- or InlB-phagosomes. Cell. Microbiol. *4*, 101–115.

Pohl, C., and Jentsch, S. (2009). Midbody ring disposal by autophagy is a post-abscission event of cytokinesis. Nat. Cell Biol. *11*, 65–70.

Pollard, T.D., and Borisy, G.G. (2003). Cellular motility driven by assembly and disassembly of actin filaments. Cell *112*, 453–465.

Sirajuddin, M., Farkasovsky, M., Hauer, F., Kühlmann, D., Macara, I.G., Weyand, M., Stark, H., and Wittinghofer, A. (2007). Structural insight into filament formation by mammalian septins. Nature *449*, 311–315.

Spiliotis, E.T., and Nelson, W.J. (2006). Here come the septins: novel polymers that coordinate intracellular functions and organization. J. Cell Sci. *119*, 4–10.

Stamm, L.M., Morisaki, J.H., Gao, L.-Y., Jeng, R.L., McDonald, K.L., Roth, R., Takeshita, S., Heuser, J., Welch, M.D., and Brown, E.J. (2003). *Mycobacterium marinum* escapes from phagosomes and is propelled by actin-based motility. J. Exp. Med. *198*, 1361–1368.

Straight, A.F., Cheung, A., Limouze, J., Chen, I., Westwood, N.J., Sellers, J.R., and Mitchison, T.J. (2003). Dissecting temporal and spatial control of cytokinesis with a myosin II Inhibitor. Science *299*, 1743–1747.

Suzuki, T., Miki, H., Takenawa, T., and Sasakawa, C. (1998). Neural Wiskott-Aldrich syndrome protein is implicated in the actin-based motility of *Shigella flexneri*. EMBO J. *17*, 2767–2776.

Tada, T., Simonetta, A., Batterton, M., Kinoshita, M., Edbauer, D., and Sheng, M. (2007). Role of Septin cytoskeleton in spine morphogenesis and dendrite development in neurons. Curr. Biol. *17*, 1752–1758.

Thurston, T.L.M., Ryzhakov, G., Bloor, S., von Muhlinen, N., and Randow, F. (2009). The TBK1 adaptor and autophagy receptor NDP52 restricts the proliferation of ubiquitin-coated bacteria. Nat. Immunol. *10*, 1215–1221.

Travassos, L.H., Carneiro, L.A.M., Ramjeet, M., Hussey, S., Kim, Y.-G., Magalhães, J.G., Yuan, L., Soares, F., Chea, E., Le Bourhis, L., et al. (2010). Nod1 and Nod2 direct autophagy by recruiting ATG16L1 to the plasma membrane at the site of bacterial entry. Nat. Immunol. *11*, 55–62.

Van Troys, M., Lambrechts, A., David, V., Demol, H., Puype, M., Pizarro-Cerda, J., Gevaert, K., Cossart, P., and Vandekerckhove, J. (2008). The actin propulsive machinery: the proteome of *Listeria monocytogenes* tails. Biochem. Biophys. Res. Commun. *375*, 194–199.

Wang, F., Graham, W.V., Wang, Y., Witkowski, E.D., Schwarz, B.T., and Turner, J.R. (2005). Interferon-$\gamma$ and tumor necrosis factor-$\alpha$ synergize to induce intestinal epithelial barrier dysfunction by up-regulating myosin light chain kinase expression. Am. J. Pathol. *166*, 409–419.

Weirich, C.S., Erzberger, J.P., and Barral, Y. (2008). The septin family of GTPases: architecture and dynamics. Nat. Rev. Mol. Cell Biol. *9*, 478–489.

Welch, M.D., Iwamatsu, A., and Mitchison, T.J. (1997). Actin polymerization is induced by Arp2/3 protein complex at the surface of *Listeria monocytogenes*. Nature *385*, 265–269.

Xie, H., Surka, M., Howard, J., and Trimble, W.S. (1999). Characterization of the mammalian septin H5: distinct patterns of cytoskeletal and membrane association from other septin proteins. Cell Motil. Cytoskeleton *43*, 52–62.

Yang, Z., and Klionsky, D.J. (2010). Eaten alive: a history of macroautophagy. Nat. Cell Biol. *12*, 814–822.

Yoshikawa, Y., Ogawa, M., Hain, T., Yoshida, M., Fukumatsu, M., Kim, M., Mimuro, H., Nakagawa, I., Yanagawa, T., Ishii, T., et al. (2009). *Listeria monocytogenes* ActA-mediated escape from autophagic recognition. Nat. Cell Biol. *11*, 1233–1240.